Generating a fractal butterfly Floquet spectrum in a class of driven SU(2) systems

Jiao Wang[1,2,*] and Jiangbin Gong[3,4,†]

[1]*Department of Physics and Institute of Theoretical Physics and Astrophysics, Xiamen University, Xiamen 361005, China*

[2]*Temasek Laboratories, National University of Singapore, Singapore 117542, Singapore*

[3]*Department of Physics and Center of Computational Science and Engineering, National University of Singapore, Singapore 117542, Singapore*

[4]*NUS Graduate School for Integrative Sciences and Engineering, Singapore 117597, Singapore*

(Received 12 June 2009; published 5 February 2010)

A scheme for generating a fractal butterfly Floquet spectrum, first proposed by Wang and Gong [Phys. Rev. A **77**, 031405(R) (2008)], is extended to driven SU(2) systems such as a driven two-mode Bose-Einstein condensate. A class of driven systems without a link with the Harper-model context is shown to have an intriguing butterfly Floquet spectrum. The found butterfly spectrum shows remarkable deviations from the known Hofstadter's butterfly. In addition, the level crossings between Floquet states of the same parity and between Floquet states of different parities are studied and highlighted. The results are relevant to studies of fractal statistics, quantum chaos, and coherent destruction of tunneling, as well as the validity of mean-field descriptions of Bose-Einstein condensates.

DOI: 10.1103/PhysRevE.81.026204 PACS number(s): 05.45.Mt, 03.75.−b

I. INTRODUCTION

Hofstadter's butterfly spectrum of the Harper model [1], first discovered in two-dimensional electron systems subject to a square lattice potential and a perpendicular magnetic field, has attracted tremendous mathematical, theoretical, and experimental interests. For an arbitrary irrational value of one system parameter, the spectrum of the Harper model is a fractal, which has been rigorously proved after decades of research on the "Ten Martini problem" [2]. As one important property of Hofstadter's butterfly spectrum, the number of its subbands depends on the arithmetic property of the flux of the magnetic field. As the magnetic flux changes smoothly and thus varies between irrational or rational numbers, the gap between the subbands shows fractal properties and will close itself infinitely times [3]. This implies that Hofstadter's butterfly spectrum contains infinite quantum phase transition points [4].

Early quantum chaos studies established that the Floquet (quasienergy) spectrum of periodically driven systems may display a fractal butterfly pattern as well [5–7]. However, the nature of the fractal Floquet spectrum is still poorly understood for three reasons. First, because the eigenphase of Floquet states is restricted to a range of 2π, understanding a Floquet spectrum associated with an infinite-dimensional Hilbert space is subtle and challenging [8]. Second, a rigorous mathematical proof about the fractal nature of a butterfly Floquet spectrum is still lacking. Third, previous findings regarding to fractal Floquet spectrum were largely limited to the so-called kicked-Harper model (a driven version of the Harper model) [5,9–12] and its variants [6,7,11–13].

Because of great interests in studies of quantum control, especially in studies of dressed matter waves [14–19], there are now promising possibilities for the engineering and simulation of driven ultracold systems with a prescribed Floquet spectrum. Reference [6] represents a recent attempt in this direction. In particular, in Ref. [6] we showed that by designing two δ-kicking sequences, the Floquet spectrum of a double-kicked-rotor system can be made to be a Hofstadter's butterfly, and the spectrum is identical with that of a kicked-Harper model when a certain parameter takes an arbitrary irrational value [13].

In this paper, we reveal yet another class of butterfly Floquet spectrum using driven SU(2) systems, which are realizable by, for example, a driven two-mode Bose-Einstein condensate (BEC). As seen below, the basic strategy is essentially an extension of our previous work [6], thus suggesting the possibility of synthesizing butterfly spectrum in many other systems that go well beyond the context of two-dimensional electron systems or the Harper-model context.

Our findings about the butterfly spectrum of driven SU(2) systems are both motivating and fascinating. First of all, as explained below, now all the three popular paradigms of quantum chaos, i.e., the kicked-rotor model, the kicked-Harper model, and the kicked-top model, are linked together, insofar as any one of them can be used to generate quantum critical systems with fractal statistics [1,20]. Second, the butterfly spectrum obtained in driven SU(2) systems is significantly different from Hofstadter's butterfly, with remarkable aspects. For example, we show that with one certain system parameter fixed the overall butterfly pattern is insensitive to the number of bosons (denoted N) in the BEC, but some detailed features depend on whether N is odd or even. This may serve as a useful guide for seeking dramatic coherence effects in a BEC. Another interesting aspect is that the butterfly spectrum contains many level crossings between states of different parities and thus many points of coherent destruction of tunneling (CDT) [15,21], with the total number of CDT points found to scale as $\sim N^{3.0}$. As an analog of quantum phase transitions in driven systems, the found butterfly pattern also contains many level crossings between same-parity eigenstates. Due to these distinctive properties, the butterfly spectrum reported here may become a test bed

*phywangj@xmu.edu.cn

†phygj@nus.edu.sg

for a number of research topics. To emphasize the remarkable differences between the butterfly spectrum found here and that associated with Harper's model, we refer to the newly found spectrum as "butterfly spectrum" instead of "Hofstadter's butterfly spectrum."

The main results of this study have been briefly reported in Ref. [22] and this paper represents a full-length description of our findings. In Sec. II we will introduce the model SU(2) system and explain the main idea behind our study. In Sec. III we study the peculiar multifractal spectral properties of the butterfly spectrum and the associated level crossings. The relevance of the underlying classical limit is also discussed in detail. To motivate possible experiments, we discuss some related issues in Sec. IV. We conclude this study in Sec. V. Appendixes A–C present some further details that may be of interest to some readers.

II. DRIVEN SU(2) MODEL

Our driven SU(2) model was motivated by a driven two-mode BEC system, proposed earlier [16,23,24] to realize the well-known kicked-top model [25] in the quantum chaos literature. In a very general form, a driven two-mode Bose-Hubbard model can be written as

$$H = f(t)\hbar(a_1^\dagger a_2 + a_2^\dagger a_1) + g(t)\hbar(a_1^\dagger a_1 - a_2^\dagger a_2)^2, \tag{1}$$

where a_i and $a_i^\dagger$ are the bosonic annihilation and creation operators for the ith mode, $f(t)$ describes the time-dependent tunneling rate between the two modes, and the $g(t)$ term describes the self-interaction between same-site bosons, whose time dependence can be achieved by Feshbach resonance induced by an additional magnetic field. Note that the total number of bosons $N=a_1^\dagger a_1+a_2^\dagger a_2$ is a conserved quantity. For a fixed N, the dimension of the Hilbert space is $N+1$. Using the Schwinger representation of angular-momentum operators, namely, $J_x=(a_1^\dagger a_2+a_2^\dagger a_1)/2$, $J_y=(a_2^\dagger a_1 - a_1^\dagger a_2)/(2i)$, and $J_z=(a_1^\dagger a_1-a_2^\dagger a_2)/2$, Eq. (1) reduces to

$$H = 2f(t)\hbar J_x + 4g(t)\hbar J_z^2. \tag{2}$$

This above Hamiltonian makes it clear that its dynamics is solely determined by the SU(2) generators J_x, J_y, and J_z. The total angular-momentum quantum number J is given by $J=N/2$. The Hilbert space can be spanned by the eigenstates of J_z, denoted $|m\rangle$, with $J_z|m\rangle=m|m\rangle$. The population difference between the two modes is given by the expectation value of $2J_z$. It is also important to note that if we exchange the indices of the two modes, then J_x is invariant, $J_z\to -J_z$, and as a result the Hamiltonian in Eq. (2) is unchanged. This reflects a parity symmetry of our model, which will be exploited below.

Consider then two specific forms of $f(t)$ and $g(t)$. In the first case $f(t)=\alpha/(2\tau)$, $g(t)=g_0\Sigma_n[\delta(t-2n\tau-\tau)-\delta(t-2n\tau)]$. The Floquet operator, i.e., the unitary evolution operator F from $2n\tau+0^+$ to $(2n+2)\tau+0^+$, is then given by

$$F = e^{i\eta J_z^2/(2J)}e^{-i\alpha J_x}e^{-i\eta J_z^2/(2J)}e^{-i\alpha J_x}, \tag{3}$$

where $\eta=4g_0N$. Interestingly, the first two or the last two factors in Eq. (3) constitute the Floquet operator for a standard kicked-top model [25]. As such our driven system here can be regarded as a "double-kicked-top model." Alternatively, if we set $g(t)=g_0/\xi$, $f(t)=\frac{\alpha}{2}\Sigma_n[\delta(t-n\tau)+\delta(t-n\tau-\xi)]$, where ξ is the time delay between the two delta kicking sequences, then the associated propagator F' from $n\tau-0^+$ to $(n+1)\tau-0^+$ is given by

$$F' = e^{-i(4g_0\tau/\xi)J_z^2}e^{i\eta J_z^2/(2J)}e^{-i\alpha J_x}e^{-i\eta J_z^2/(2J)}e^{-i\alpha J_x}. \tag{4}$$

Under the special condition $4g_0\tau/\xi=2k\pi(8k\pi)$ for integer J (half-integer J), where k is an integer, the factor $e^{-i(4g_0\tau/\xi)J_z^2}$ is unity in the $(2J+1)$-dimensional Hilbert space and hence F' becomes identical with F. Based on this, one now has two different scenarios for realizing F, the key operator to be analyzed in this paper.

To explain our motivation of considering the operator F, let us consider the $|m\rangle$ representation. In that representation the third factor $e^{-i\eta J_z^2/(2J)}$ of F equals $e^{-i\eta m^2/(2J)}$, which is a pseudorandom number for irrational η/J. Interestingly, the first factor of F however effectively induces a time reversal of the third factor and thus partially cancels this pseudorandom phase. Indeed, using the SU(2) algebra [26], the product of the first three factors of F in Eq. (3) is given by

$$e^{i\eta J_z^2/(2J)}e^{-i\alpha J_x}e^{-i\eta J_z^2/(2J)} = \exp[-i\alpha\{(J_x/2 + iJ_y/2) \times e^{i[\eta(2J_z+1)/(2J)]} + \text{c.c.}\}]. \tag{5}$$

This shows that the η-dependent term entering into F becomes $e^{i[\eta(2J_z+1)/(2J)]}$, which is always a quasiperiodic number $e^{i[\eta(2m+1)/(2J)]}$ in the $|m\rangle$ representation. According to our early work [27], such a partial cancellation of quasirandom dynamical phases implies intriguing spectral properties.

For later discussion we also study the classical limit of F. To that end we consider scaled variables $x=J_x/J$, $y=J_y/J$, and $z=J_z/J$. Evidently, the three operators x, y, and z also satisfy the angular-momentum algebra, but with an effective Planck constant $\hbar_{\text{eff}}\equiv 1/J$. Taking the $\hbar_{\text{eff}}\to 0$ limit with fixed η and α, the classical dynamics associated with F can be obtained, with variables x, y, and z restricted on a unit sphere. Because $\eta=4g_0N$, this classical limit with fixed η requires $N\to+\infty$ and $g_0\to 0$. This condition is apparently equivalent to that appearing in a standard mean-field limit of the driven BEC.

In addition to the system defined by F, we also consider one of its interesting variants,

$$F_{xy} = e^{i\eta J_z^2/(2J)}e^{-i\alpha J_x}e^{-i\eta J_z^2/(2J)}e^{-i\alpha J_y}, \tag{6}$$

which is different from F in the last factor, i.e., $e^{-i\alpha J_x}$ in F is replaced by $e^{-i\alpha J_y}$. As seen below, such a variant may induce considerable changes in the spectral properties.

III. DETAILED ASPECTS OF THE BUTTERFLY SPECTRUM

A. Multifractal properties

In the $|m\rangle$ representation, the matrix elements of the operator F can be evaluated in a straightforward manner. Diagonalizing F numerically then yields its spectrum. Figure 1

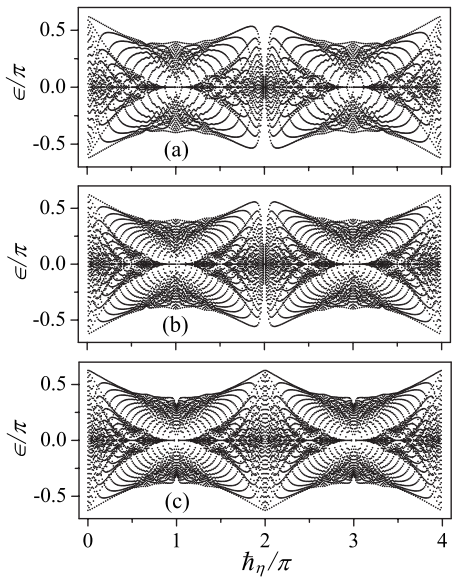

FIG. 1. The eigenphase spectrum (denoted ϵ) of the Floquet operator F in Eq. (3). $J=20$ in (a), 30 in (b), and 30.5 in (c). $\alpha/\hbar_{\text{eff}}=1$ in all panels. Beautiful butterfly patterns are clearly recognized. Analogous result for $J=100$ can be found in Ref. [22].

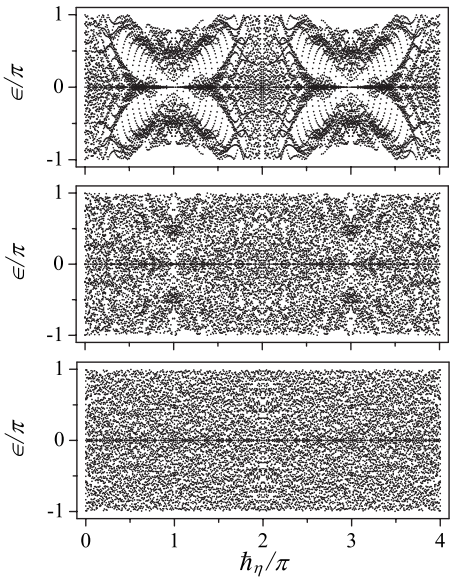

FIG. 2. The dissolving of the butterfly pattern of the eigenphase spectrum of the Floquet operator F in Eq. (3). In all the panels $J=30$. From top to bottom: $\alpha/\hbar_{\text{eff}}=3$, 6, and 10, respectively. This process resembles that observed in the kicked-Harper model [5].

shows the typical eigenphase spectrum of F vs $\hbar_\eta \equiv \eta\hbar_{\text{eff}} = \eta/J = 8g_0$, for $J=20$, 30, 30.5, and $\alpha/\hbar_{\text{eff}}=\alpha J=1$. Because the spectrum of F is invariant if $\hbar_\eta \to \hbar_\eta + 4\pi$ (see the proof in Appendix A), we set $\hbar_\eta \in [0, 4\pi)$. Though in Fig. 1 the involved Hilbert space is rather small, spectacular butterfly patterns are already obtained. Their reflection symmetry with respect to $\hbar_\eta = 2\pi$ is also clearly seen, a fact proved in Appendix B. The found butterfly patterns in Fig. 1 resemble the famous Hofstadter's butterfly, but also present remarkable differences in several aspects. First, if we take a vertical cut of the butterfly patterns in Fig. 1, the spectrum is not found to present any large gaps. Second, the butterfly patterns shown in each panel of Fig. 1 possess a double-butterfly structure, with each butterfly covering a 2π range of $\hbar_\eta$. This double-butterfly structure is somewhat analogous to the spectrum of a Harper-like effective Hamiltonian considered in Ref. [12]. More interestingly, though Figs. 1(b) and 1(c) has more levels than Fig. 1(a), the overall outline of the double-butterfly structure is seen to be insensitive to J for fixed $\alpha/\hbar_{\text{eff}}=\alpha J$. Indeed, in Fig. 1(c) of Ref. [22] we also presented the spectrum for a much larger J value, i.e., $J=100$, and again similar outline of the butterfly spectrum is obtained. Qualitatively this is because when $\alpha/\hbar_{\text{eff}}=\alpha J$ is fixed, the phase range of the second and fourth factors of F is also fixed. By contrast, for a fixed value of J but for other not too large values of α, the qualitative features of the butterfly spectrum remain, but at different scales. For very large values of α (e.g., $\alpha/\hbar_{\text{eff}}>10$), the butterfly pattern for a fixed value of J will gradually dissolve, as seen in Fig. 2. This dissolving process of a butterfly spectrum is similar to that seen in the kicked-Harper model [5].

Some detailed features of the spectrum are also noteworthy. For example, it is observed that the spectrum collapses to one point for $\hbar_\eta = 2\pi$, if and only if J is an integer. This can be explained as follows. If J is an integer and if $\hbar_\eta = 2\pi$, then in the $|m\rangle$ representation,

$$e^{-i\eta J_z^2/(2J)} = e^{-i\pi m^2} = e^{-i\pi m} = e^{-i\pi J_z}. \tag{7}$$

So in this case $e^{-i\eta J_z^2/(2J)}$ is equivalent to a rotation of π around the z axis, and hence the first three factors of F exactly cancel its last factor. This cancellation will not occur if J is a half-integer, i.e., if N is odd. Later we will return to this intriguing difference between odd-N and even-N cases.

We have also examined the statistical behavior of the found butterfly spectrum. To have good statistics we consider a much larger $J=2999$. Figure 3(a) presents the cumulative level density $N(\epsilon)$ for a representative value of $\hbar_\eta$. It is seen that $N(\epsilon)$ is highly irregular, but does not show any clear flat steps. This is consistent with our early observation that no large gap exists in the spectrum. Figures 3(b)–3(d) show the associated coarse-grained level distribution $P(\epsilon)$ at three different scales. Evidently, $P(\epsilon)$ has a fascinating self-similar property. $P(\epsilon)$ is evaluated by scanning the spectrum in a series of bins of width Δ: $P(\epsilon)=n_i/[(2J+1)\Delta]$ for $\epsilon \in [i\Delta,(i+1)\Delta)$, where n_i is the level number in this ϵ range. In generating Figs. 3(b)–3(d) we have set $\Delta=0.02\pi$.

The self-similarity shown in Figs. 3(b)–3(d) motivates us to quantitatively characterize the spectrum via the generalized fractal dimension D_q [28],

$$D_q = \frac{1}{q-1}\lim_{\Delta\to 0}\frac{\log\sum_i p_i^q}{\log \Delta}, \tag{8}$$

where $p_i=n_i/(2J+1)$ is the probability associated with the ith bin. For a given spectrum D_q can be computed by the linear regression of $\log\Sigma_i p_i^q$ versus $\log\Delta$ over an appropriate range of Δ. The results of D_q for the operator F are shown in Fig. 3(e), where the Δ range of $\Delta \in [0.006, 0.6]$ is considered. We adopt this Δ range with two considerations: on one hand it should be large enough to capture the fluctuations at various

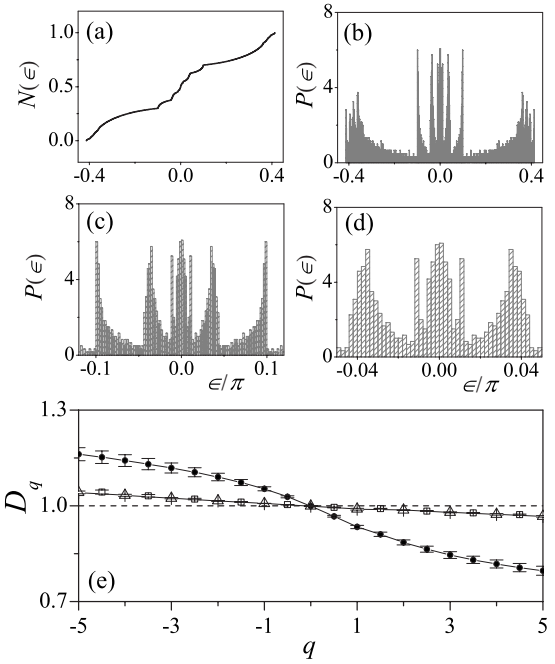

FIG. 3. Cumulative Floquet state density (a) and the coarse-grained state density distribution (b)–(d) at different scales for the operator F with $\hbar_\eta=(\sqrt{5}-1)\pi/2$, $\alpha/\hbar_{\text{eff}}=1$, and $J=2999$. Panel (e) shows the generalized fractal dimension D_q of the spectrum (see text for the evaluation method). Solid dots and open squares are for the spectra of F and the standard kicked-top model [25], respectively. As a comparison the open triangles are for the D_q evaluated over a sequence of $2J+1$ random numbers distributed uniformly in $(0,2\pi)$, which agree very well with the results of the standard kicked-top model. The dashed line ($D_q=1$) is for reference.

scales and on the other hand the errors of D_q estimated in the linear regression processes should be as small as possible. In all our calculations of D_q, the errors of D_q thus obtained are less than 2% [see error bars in Fig. 3(e)]. As expected from the $N(\epsilon)$ result in Fig. 3(a) we have $D_0=1$. However D_q for $q\neq 0$ clearly shows that the spectrum has multifractal properties. For the sake of comparison, Fig. 3(e) also shows the D_q results for the standard kicked-top model [25] (i.e., considering an operator comprising only the first two factors of F) with the same values of parameters η and α. In clear contrast it remains close to unity but slightly deviates with increasing $|q|$. It should be noted that in generating Fig. 3 the whole spectrum of the system F and that of the standard kicked-top model has been taken into account; but further numerical analysis have confirmed that in both cases when the spectrum of the eigenstates of odd and even parities are considered separately, the corresponding results of D_q are identical to those of the whole spectrum (see Fig. 3) within the evaluated errors.

In order to understand the slight deviations of D_q from unity for $q\neq 0$ in the standard kicked-top model, we performed the calculations of D_q of a random sequence. It consists of 5999 random numbers, of the same number of total levels for $J=2999$ in both previous cases, and the random numbers are generated from a uniform distribution over $(0,2\pi)$. As can be seen in Fig. 3(e), the obtained D_q agree

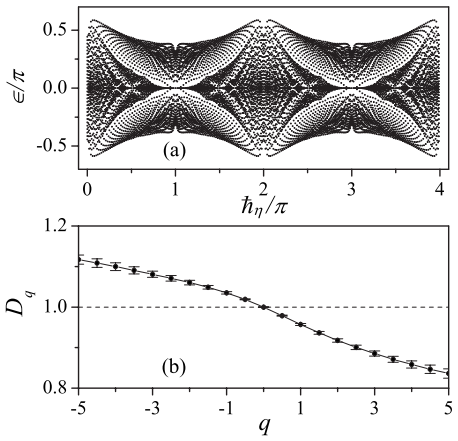

FIG. 4. (a) Eigenphase spectrum of the Floquet operator F_{xy} [Eq. (6)] for $J=30$. (b) The corresponding fractal dimension D_q computed for $J=2999$ and $\hbar_\eta=(\sqrt{5}-1)\pi/2$ (solid dots). The dashed line ($D_q=1$) is for reference. $\alpha/\hbar_{\text{eff}}=1$ in both panels.

with those of the standard kicked-top model perfectly. This agreement suggests that with the given parameters α and η, the standard kicked-top model is classically near-integrable and quantum mechanically its spectrum follows the Poisson statistics. This is also confirmed by our numerical analysis (not shown here). On the other hand, for a true uniform random sequence one expects $D_q=1$; hence the deviations of D_q from unity as observed in Fig. 3(e) can be safely linked with a finite-size effect. Indeed, we have verified that as the length of the random sequence is increased the deviations of D_q from unity approaches zero asymptotically.

Based on the results of D_q for the system F (also considering the errors of D_q, together with the possible finite-size effect for the system size $J=2999$, as suggested by the above-mentioned random sequence analysis), we tend to conjecture that the butterfly patterns found in the spectrum of F may contain true fractals in the limit of $J\to+\infty$. It will be of importance to devote more efforts to this conjecture. However, our other analysis suggests that a direct numerical check of our conjecture would require analogous calculations for $J\sim 10^5$, which is far beyond our current computational capacities.

We have also studied the F_{xy} model defined above, obtaining a similar multifractal butterfly spectrum, as shown in Fig. 4(a). Interestingly, despite that the outline of the butterfly spectrum of F_{xy} is much similar to that for F, careful investigations reveal considerable differences between the butterfly spectrum of F_{xy} and that for F. For example, the fractal dimension D_q shown in Fig. 4(b) for F_{xy} is similar to, but slightly larger (smaller) than, that of F for $q>0$ ($q<0$). It is found that this is because the gaps in the butterfly spectrum of F_{xy} are more densely filled than that of F [compare Figs. 4(a) and 1(b)]. In the next subsection we will point out an even more fundamental difference between these two systems.

B. Level crossings

In this subsection we study the level crossings in the butterfly spectrum as the parameter $\hbar_\eta$ varies. Note first that due

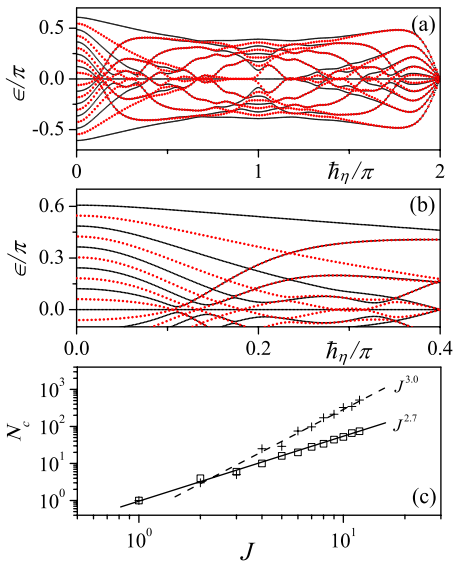

FIG. 5. (Color online) (a) Level crossings between ten even-parity states (solid) and nine odd-parity states (dotted) for $J=10$ and $\alpha/\hbar_{\text{eff}}=1.0$. (b) A magnification of one part of (a). (c) The number of level crossings versus J, for $\hbar_\eta \in [0,4\pi)$ and $\alpha/\hbar_{\text{eff}}=1.0$. The cross (square) symbols are for crossings between different-parity (same-parity) states and the fitting suggests a power law scaling $J^{3.0}(J^{2.7})$.

to the above-mentioned symmetry $\langle m|F|n\rangle=\langle -m|F|-n\rangle$, the eigenstates of F can be classified into J eigenstates of odd parity and $J+1$ states of even parity. As such, we should investigate the crossings between different-parity states and between same-parity states. In either case, computationally it is found that the minimal distance in $\hbar_\eta$ between two level crossings decreases sharply with J. So even for a rather small $J\sim 10$ it is already numerically demanding to identify all the level crossings.

As an example Figs. 5(a) and 5(b) present the typical level crossing behavior for $J=10$. The Floquet states are seen to cross each other frequently, between different-parity states and between same-parity states. Both types of level crossings turn out to be of vast interest. For the first type, at a crossing point an arbitrary superposition of two crossing states of different parities remains an eigenstate but generally breaks the parity symmetry. So if such a superposition state is used as the initial state, the ensuing dynamics will maintain a nonzero population difference between the two modes forever [16,17]. This makes it clear that the first type of level crossings give rise to the seminal CDT phenomenon [15,21] that has attracted broad experimental and theoretical interests. It should be pointed out that in some regimes of $\hbar_\eta$, to the naked eyes two curves of opposite parities in Figs. 5(a) and 5(b) are almost on top of each other. As a result many CDT points are found in these regimes. Note also that the CDT-induced population trapping is fundamentally different from the well-known self-trapping effect on the mean-field level. Indeed, the CDT effect here depends on η and J, whereas mean-field self-trapping is transient and independent of J.

Now turning to the second type of level crossings, they come as a surprise because avoided crossings between same-parity states, rather than true level crossings, are generally

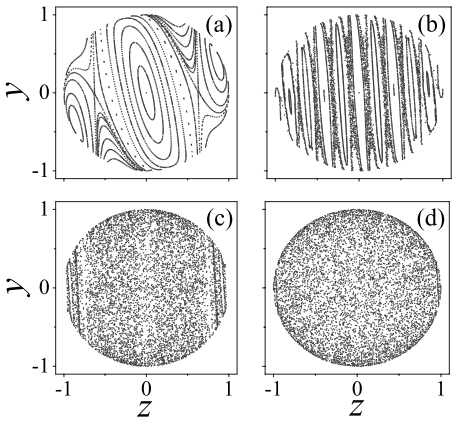

FIG. 6. Poincaré surfaces of section (with $J_x>0$) of the classical or mean-field limit of F in Eq. (3), with $\alpha=0.05$ [same as in Fig. 1(a)], $\eta=5$ in (a), 30 in (b), 75 in (c), and 100 in (d).

anticipated for classically nonintegrable systems (see Figs. 6 and 7). The second type of crossings therefore suggests the uniqueness (e.g., some effective local "symmetry") of F whose matrix elements in the $|m\rangle$ representation are quasiperiodic. Recalling the above-mentioned extreme example where all levels cross at $\hbar_\eta=2\pi$ for integer J, we expect that special arithmetic properties of $\hbar_\eta$ play a key role in both types of level crossings.

Careful checks are made to ensure that the same-parity level crossings observed here are not avoided crossings with a very small gap. For example, we examined the crossing behavior for small J, where analytical studies become possible. In particular, for $J=2$, using Wigner's rotational matrices to express the second and fourth factors of F, we can analytically prove that there must be true level crossings between two odd-parity states, at $\hbar_\eta=2\pi/3$ and $\hbar_\eta=10\pi/3$, regardless of the value of α. This is fully consistent with our numerical finding. Details for this case are presented in Appendix C. This further confirms that the number theory properties of $\hbar_\eta$ are responsible for the same-parity level crossings. As another check, we also studied the level crossing

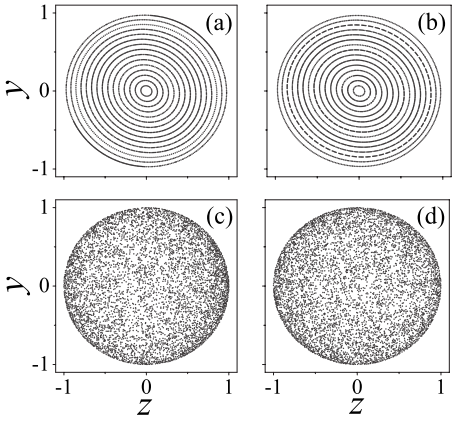

FIG. 7. Same as in Fig. 6 but $\alpha=0.1/3$ in (a) and $\alpha=1/3$ in (b) with $\eta=0.06\pi$; $\alpha=0.1/3$ in (c) and $\alpha=1/3$ in (d) with $\eta=0.06\pi+120\pi$. Quantum mechanically, for $J=30$, cases (a) and (c), or cases (b) and (d), share the same spectrum due to the spectral symmetry under $\hbar_\eta\rightarrow\hbar_\eta+4\pi$.

behavior in the butterfly spectrum of F_{xy}. Therein we only obtain avoided crossings between all the eigenphases (see also Fig. 9 in Appendix C). For $J \leq 12$ and for the same parameters as in Fig. 5(c), the typical gaps of the avoided level crossings in the spectrum of F_{xy} are found to be $>10^{-6}$, many orders of magnitude larger than the accuracy of our eigenphase calculations (10^{-13}). This "control case" hence indirectly supports our observation of same-parity level crossings for F.

By obtaining all the level crossings in the butterfly spectrum of F with high accuracy for $J \leq 12$, we obtain in Fig. 5(c) that the number of CDT points contained in the butterfly patterns scales as $J^{3.0}$ and the number of same-parity crossings scales as $J^{2.7}$. In either case, the number of crossings divided by the total number of levels ($\sim J$) or divided by the total number of level pairs ($\sim J^2$) diverges as $J \to +\infty$. In particular, we assert that as N goes to infinity, on average each pair of Floquet states in a butterfly pattern see infinite CDT points.

C. Relevance of the classical limit

An interesting question is what implications the classical dynamics may have on the fractal spectrum observed in the F system. To this end we investigate the classical limit of F defined above. Numerical studies indicate that classically the system can be governed by both regular and chaotic motions, depending on the two system parameters η and α. In general, for a fixed α, as η increases the classical dynamics undergoes a transition from being regular to being chaotic. As an example Fig. 6 presents the phase space structure of the classical limit of F with $\alpha=0.05$ and an increasing η.

Such a classical regular-to-chaos transition lacks a quantum counterpart in the butterfly spectrum shown in Figs. 1 and 2, whose characteristics can be much similar for radically different values of η. Indeed, the quantum Floquet spectrum is periodic in η with a period $4J\pi$ (see Appendix A). Therefore, upon quantization the regular or chaotic nature of the classical dynamics may not necessarily be reflected in the spectrum and hence can be irrelevant to the quantum dynamics.

Interestingly, the regular-to-chaos transition in the classical dynamics is not even connected to the dissolving of the butterfly spectrum (see Fig. 2). As an example, let us examine such a dissolving process for $J=30$ from $\alpha/\hbar_{\text{eff}}=1$ [Fig. 1(b)] to $\alpha/\hbar_{\text{eff}}=3$, 6, and 10 (Fig. 2), corresponding to $\alpha=0.1/3$, 0.1, 0.2, and 1/3, respectively. Consider the spectrum along the vertical cuts of these figures at $\hbar_\eta/\pi=2\times10^{-3}$, i.e., $\eta=0.06\pi$. It is found that in spite of the drastic changes of the spectrum in this dissolving process, the dynamics in the classical limit remains regular all the way from $\alpha=0.1/3$ to 1/3 [see Figs. 7(a) and 7(b)]. On the other hand, due to the 4π periodicity of the quantum spectrum in $\hbar_\eta$, we expect the same dissolving process if we change η from 0.06π to $0.06\pi+120\pi$. However, the corresponding classical dynamics is now completely chaotic [see Figs. 7(c) and 7(d)]. Hence the dissolving of the butterfly spectrum is unrelated to the classical dynamics. This is in contrast to the kicked-Harper model, where the dissolving of Hofstadter's butterfly was somewhat connected to the classical regular-to-chaos transition [5].

The little relevance of the classical limit in understanding the butterfly spectrum also makes our model markedly different from the conventional kicked-top model as a paradigm for quantum chaos. We believe that such a lack of classical-quantum correspondence is a result of a built-in feature of our SU(2) model. That is, our strategy for generating the fractal spectrum is based on a partial cancellation of quasirandom dynamical phases [see Eq. (5)], and this partial cancellation of quantum phases is a pure quantum feature with no classical analog. To double check this we also studied the classical dynamics of the F_{xy} model and reached the same conclusion.

D. Generating a fractal-spectrum family

In the previous subsection we have studied the butterfly spectrum associated with F. Here we point out that the butterfly spectrum of F is just one member of a whole butterfly-spectrum family. Let us restrict ourselves to cases of integer J and consider the following function:

$$g(t) = \sum_n [g_0 \delta(t - 2n\tau - \tau) + \tilde{g}_0 \delta(t - 2n\tau)],$$

instead of that used in generating F as in Eq. (3). Here $\tilde{g}_0 = (\frac{\pi}{2} \cdot \frac{\nu}{\mu} - g_0)$ and μ and ν are two integers sharing no common factors. We can then obtain an extended class of Floquet operators

$$F^{(\nu/\mu)} \equiv e^{i2\pi J_z^2 \nu/\mu} e^{i\eta J_z^2/(2J)} e^{-i\alpha J_x} e^{-i\eta J_z^2/(2J)} e^{-i\alpha J_x} = e^{i2\pi J_z^2 \nu/\mu} F. \tag{9}$$

We also note that $F^{(\nu/\mu)}$ can be obtained if we set $4g_0\tau/\xi = 2\pi\nu/\mu$ in Eq. (4). Obviously, F corresponds to the special case of $\nu=\mu=1$.

In the double-kicked-rotor model considered in Ref. [7], one can construct analogous operators by employing high-order quantum resonances, where ν/μ indicates the resonance order. For each choice of ν/μ a certain type of fractal spectrum can be generated. An example for $\nu/\mu=1/2$, the so-called antiresonance condition, can be found in Ref. [7] (see Fig. 3 therein).

Interestingly, the spectrum of $F^{(\nu/\mu)}$ defined in Eq. (9) also forms a fractal-spectrum family, with the outline of each butterfly roughly similar to its relative in the double-kicked-rotor model considered in Ref. [7]. We also find that for integer J, the peculiar spectral characteristics of F discussed above can be maintained in the spectrum of $F^{(\nu/\mu)}$. For example, we have investigated thoroughly the case of $\nu/\mu = 1/2$ and obtained that (1) D_q curve is qualitatively the same as that for F; i.e., $D_0=1$ and $|1-D_q|$ increases as $|q|$ increases; (2) level crossings between eigenstates of the same or different parities can occur; and (3) the dynamics in the classical limit is also irrelevant in understanding the quantum spectrum. Similarly, the spectral properties of F_{xy} are also found to be similar to its high-order extension $F_{xy}^{(\nu/\mu)} \equiv e^{i2\pi J_z^2 \nu/\mu} F_{xy}$. The possibility of constructing such a butterfly-spectrum family provides further support that our

strategy for generating a fractal Floquet spectrum in driven quantum systems is quite general.

IV. DISCUSSION

Experimental confirmation of a butterfly Floquet spectrum in driven systems is challenging. In the case of the kicked-Harper model, there have been a few experimental proposals but so far the kicked-Harper model has not been experimentally realized. The double-kicked-rotor model proposed in Ref. [6] opens up a new opportunity. However, in atom-optics realizations of the kicked-rotor model, a dilute cold gas in a kicking one-dimensional optical-lattice potential is required, the quasimomentum spread of the initial state should be sufficiently narrow, and the interaction between the atoms should be negligible. By contrast, in the present study, we rely on an interacting cold gas distributed on two modes, and there is no quasimomentum issue. Moreover, because the effective Planck constant $\hbar_\eta$ is simply given by $8g_0$, by tuning the atom-atom interaction constant alone we may scan the butterfly spectrum already. These advantages make the systems proposed in this study a promising alternative for possible experimental realizations of a butterfly Floquet spectrum.

There are also other motivations for further theoretical and experimental studies of our model. First, because the found butterfly spectrum collapses at $\hbar_\eta=2\pi$ (or $g_0=\pi/4$) for integer J, one may experimentally determine if N is even or odd by scanning the dynamics in the neighborhood of $g_0=\pi/4$. Note that detecting the even-odd properties of N is impossible in the mean-field dynamics of a BEC, and such a topic is already under investigation in Refs. [17,29] via other mechanisms. Similarly, one may study the CDT points to reveal non-mean-field effects. Second, it is now of great interest, both experimentally and computationally, to revisit early results of how a multifractal spectrum can be manifested in time-dependent properties [30]. Third, noticing that recently dissipative two-mode BECs have attracted considerable attention [31], it seems interesting to study dissipation effects on a butterfly spectrum. Fourth, in the time-periodic driven systems, (multi-)fractal may characterize the systems in different aspects other than the spectrum. For example, it has been revealed that in the kicked-rotor model with absorbing boundary conditions the quantum survival probability can be well related, both theoretically and numerically, to the (multi-)fractal parametric fluctuations [32]. It would be interesting to investigate if the similar (multi-)fractal transporting fluctuations exist in our system and to what extent they can be understood with the established theory.

Experiments of our model system with a small J can be also interesting. For example, for the $J=2$ case we have found that the F operator is an identity matrix in the odd-parity subspace at $\hbar_\eta=2\pi/3$ and $10\pi/3$ (see Appendix C). Such cases may be used to extract the value of g_0 to a good precision. They may be also useful to explore the implication of level crossings between same-parity states.

We next discuss how to experimentally confirm a butterfly spectrum. Certainly, a Floquet spectrum cannot be directly measured. However, in principle there is a standard procedure to invert the Floquet spectrum from the dynamics. This involves quantum state reconstruction of the evolving two-mode BEC. That is, after each period of the driving field, enough measurements on different observables are to be made to reconstruct the state of the evolving two-mode BEC. This is possible because quantum state reconstruction of a BEC is currently a very active and fruitful area. This state reconstruction is not expected to be prohibitively demanding if N is relatively small. With the quantum states at different times reconstructed, then by making a fast-Fourier-transformation (FFT) of the time-evolving state, the Floquet spectrum may be obtained.

We point out that there is no need to follow the dynamics for very long in order to resolve a butterfly spectrum. Let us assume that the wave functions are already reconstructed by sufficient measurements at integer multiples of the driving period τ. To examine how many periods are needed for obtaining the butterfly spectrum from experiments, we consider an example where the initial state is chosen as $|m=10\rangle$ for $J=20$. Using the same parameters as in Fig. 1(a), and using the time-evolving states after $n=32$, 64, 128, 256, 512, and 1024 kick pairs, the spectrum obtained via FFT are shown in Fig. 8. It is seen that a few hundred kicks can be good enough to resolve the shape of a butterfly spectrum relatively well. If, as discussed in the following, the time scale of the kicking period is chosen to be 10^{-5} s, then this means that the required duration to follow the dynamics in an experiment is around 0.01 s.

Finally, let us comment on the parameter ranges we have chosen. First of all, to ensure that a wide regime of the found butterfly spectrum can be visited in a real system, a tunable g_0 is required, and its characteristic value should be ~ 1. Let g_c be the self-interaction constant of a static two-mode BEC. A reasonable range of g_c/f (f is the tunneling rate) is from 10^{-3} to 10^{-2} for a two-mode BEC in a double-well potential [23]. With the first realization of F in mind and for $\alpha J=1$ and $J=10$, we have $g_c/f=2\tau g_c/\alpha$, and that $2\tau g_c$ ranges from 10^{-4} to 10^{-3}. This indicates that $g_0/(\tau g_c)$ should be around 10^3-10^4. If the value of g_c (in SI unit of frequency) is about 50 s^{-1} (a value considered in [23]), we have that τ is in the range of 10^{-6} s to 10^{-5} s. Considering other realizations of a two-mode BEC might lead to different characteristic values of τ and $g_0/(\tau g_c)$.

V. CONCLUSION

We have presented a strategy for generating a fractal butterfly Floquet spectrum in a class of driven SU(2) systems. The essence of this strategy is to partially cancel the quasirandom dynamical phases in the time evolution and then induce intriguing spectral properties. The success of such a strategy in both this work and our early work [6] treating a double-kicked-rotor model indicates its wide applicability. As such, butterfly Floquet spectrum is expected to occur in many driven quantum systems that can go well beyond the context of two-dimensional electron systems or the Harper-model context. A butterfly spectrum thus obtained may also differ significantly from Hofstadter's butterfly.

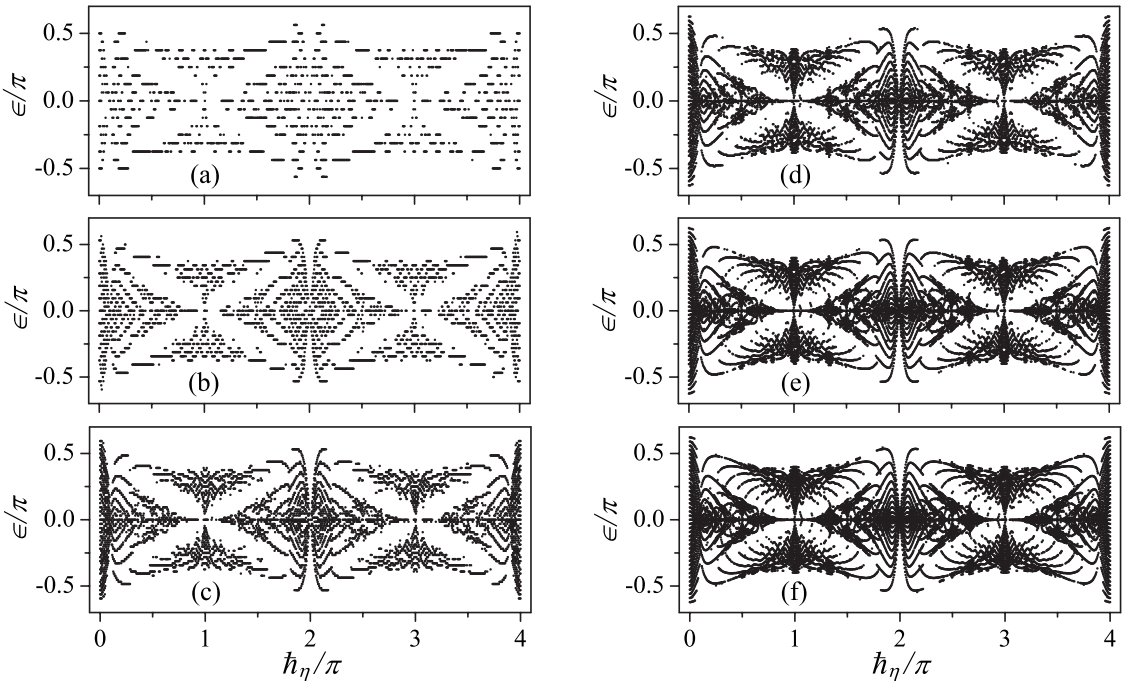

FIG. 8. Eigenphase spectrum of the Floquet operator F for $J=20$ and $\alpha/\hbar_{\text{eff}}=1$, retrieved via an FFT of the sequence $\{\langle\phi(0)|F^n|\phi(0)\rangle, n=1,\ldots,N\}$ with the sequence length $N=32$ (a), 64 (b), 128 (c), 256(d), 512 (e), and 1024 (f). The initial condition is given by $|\phi(0)\rangle=|10\rangle$ as an example.

Detailed aspects of the butterfly spectrum in driven SU(2) systems are also examined. The level crossing features in the butterfly spectrum, especially its connection with coherent destruction of tunneling, and the surprising observation of level crossings between same-parity states, are emphasized. The sensitivity of the butterfly spectrum on the even-odd properties of the number of particles is also highlighted. Many further questions can be asked and we believe that our driven SU(2) model will be relevant to a number of related research topics, including fractal statistics, quantum chaos, quantum control, and the validity of mean-field descriptions of Bose-Einstein condensates.

The conventional system for understanding a butterfly Floquet spectrum is the kicked-Harper model. Therein the quantization rule varies with the boundary condition adopted [33] and a compact toroidal phase space arises only if the Planck constant assumes special values [9]. A general treatment of the kicked-Harper model leads to a band structure that often complicates the issue. By contrast, the phase space structure in our driven SU(2) model is necessarily on a sphere [25], with no arbitrariness in quantization and no band structure in the spectrum. For these reasons we hope that the butterfly Floquet spectrum discovered here can stimulate future studies on general implications of a fractal Floquet spectrum. Combining this work with our early study [6], we have that three paradigms of quantum and classical chaos, i.e., the kicked-rotor model, the kicked-Harper model, and the kicked-top model, are linked all together because any one of the three contexts can be used to generate quantum critical systems with a fractal Floquet spectrum.

ACKNOWLEDGMENTS

We thank Professor C.-H. Lai for his kind support and for making this collaborative work possible. J.G. was supported by WBS (Grant No. R-144-050-193-101/133) and the NUS "YIA" (Grant No. R-144-000-195-101). J.W. acknowledges support from National Natural Science Foundation of China (Grant No.10975115) and DSTA of Singapore (Agreement No. POD0613356).

APPENDIX A: 4π PERIODICITY OF F IN $\hbar_\eta$

Letting $U(\hbar_\eta)\equiv e^{\eta J_z^2/(2J)}$, the operator F can be written as $F(\hbar_\eta)=U(\hbar_\eta)e^{-i\alpha J_x}U^\dagger(\hbar_\eta)e^{-i\alpha J_x}$. It can be shown that

$$U(\hbar_\eta+4\pi)=\pm U(\hbar_\eta), \tag{A1}$$

hence $F(\hbar_\eta+4\pi)=F(\hbar_\eta)$. To show the above equality let us consider the representation using the eigenstates of J_z, i.e., $J_z|m\rangle=m\hbar|m\rangle$, in which U is diagonalized and $\langle m|U(\hbar_\eta+4\pi)|m\rangle=e^{i(\eta+4J\pi)m^2/(2J)}$, resulting in $U(\hbar_\eta+4\pi)=U(\hbar_\eta)$ if J is an integer, and $U(\hbar_\eta+4\pi)=-U(\hbar_\eta)$ if J is a half-integer. In the latter case as $U^\dagger(\hbar_\eta+4\pi)=-U^\dagger(\hbar_\eta)$, which contributes a second minus sign, we again have $F(\hbar_\eta+4\pi)=F(\hbar_\eta)$.

APPENDIX B: SPECTRUM SYMMETRY OF F UNDER $\hbar_\eta\rightarrow-\hbar_\eta$

Consider first the F operator and its eigenfunction $|\psi\rangle$ with

$$F(\hbar_\eta)|\psi\rangle=e^{-i\omega}|\psi\rangle. \tag{B1}$$

Multiplying $e^{-i\hbar_\eta J_z^2/2}e^{-i\alpha J_x}$ to both sides of the above eigenfunction equation and defining that $|\psi'\rangle \equiv e^{-i\hbar_\eta J_z^2/2}e^{-i\alpha J_x}|\psi\rangle$, then we have

$$F(-\hbar_\eta)|\psi'\rangle = e^{-i\omega}|\psi'\rangle. \tag{B2}$$

Hence, comparing Eqs. (B1) and (B2) one sees that the spectrum of $F(\hbar_\eta)$ is identical with that of $F(-\hbar_\eta)$.

Combining this result with the 4π periodicity of F in $\hbar_\eta$, one obtains that the butterfly spectrum of F has a reflection symmetry with respect to $\hbar_\eta = 2\pi$.

APPENDIX C: LEVEL CROSSINGS BETWEEN TWO ODD-PARITY STATES OF F FOR $J=2$

The arithmetic properties of $\hbar_\eta$ can cause surprising and frequent level crossings between same-parity eigenstates of F. To understand this counterintuitive result we consider a simple case with $J=2$. Numerically we observe level crossings between two odd-parity states at $\hbar_\eta = 2\pi/3$ and $\hbar_\eta = 10\pi/3$ besides that at $\hbar_\eta = 2\pi$ [see Fig. 9(a) for $\alpha/\hbar_{\text{eff}}=1$]. Here we give a mathematical proof that this is indeed the case, thus supporting the numerically observed level crossings in general. Note that our approach can be extended to other cases as well.

We first note that each of the four factors of F preserves the parity. So if we consider the odd-parity subspace only, then each of the four factors can be reduced to a 2×2 matrix because the odd-parity subspace is two dimensional for $J=2$. Specifically, we consider the following basis states:

$$|\tilde{2}\rangle \equiv (|2\rangle - |-2\rangle)/\sqrt{2},$$

$$|\tilde{1}\rangle \equiv (|1\rangle - |-1\rangle)/\sqrt{2}.$$

In this representation, the factor $e^{i\hbar_\eta J_z^2/2}$ and $e^{-i\hbar_\eta J_z^2/2}$ for $\hbar_\eta = 2\pi/3$ are given by

$$U \equiv \begin{pmatrix} e^{i4\pi/3} & 0 \\ 0 & e^{i\pi/3} \end{pmatrix}$$

and $U^\dagger$, respectively.

In order to get the matrix expression of F, we need to get the analytical expression for the factor $e^{-i\alpha J_x}$. Fortunately, this can also be done by using Wigner's rotational matrices [34]. Denoting $D^2_{m'm}$ as Wigner's expression for the rotational matrix, we have

$$D^2_{m'm} = \langle m'|e^{-i\alpha J_y}|m\rangle. \tag{C1}$$

What we need is the matrix $\langle m'|e^{-i\alpha J_x}|m\rangle$, which is related to $D^2_{m'm}$ by

$$\langle m'|e^{-i\alpha J_x}|m\rangle = i^{m'-m}D^2_{m'm}. \tag{C2}$$

Using the explicit expressions of the rotational matrix $D^2_{m'm}$ given in [34], we obtain

$$\langle 2|e^{-i\alpha J_x}|2\rangle = \cos^4(\alpha/2),$$

$$\langle 2|e^{-i\alpha J_x}|-2\rangle = \sin^4(\alpha/2),$$

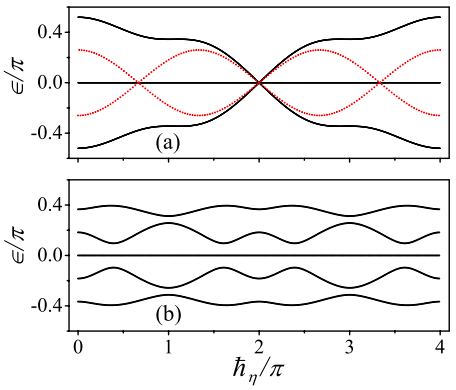

FIG. 9. (Color online) The eigenphase spectrum of the Floquet operator F (a) and F_{xy} (b) for $J=2$ and $\alpha/\hbar_{\text{eff}}=1$. In (a) the two eigenphases of odd parity (dotted) cross at $\hbar_\eta = 2\pi/3$, 2π, and $10\pi/3$, while the three eigenphases of even parity (solid) only cross at $\hbar_\eta = 2\pi$. As a contrast, the spectrum of F_{xy} displays avoided crossings instead.

$$\langle 1|e^{-i\alpha J_x}|1\rangle = [1+\cos(\alpha)][2\cos(\alpha)-1]/2,$$

$$\langle 1|e^{-i\alpha J_x}|-1\rangle = -[1+2\cos(\alpha)][1-\cos(\alpha)]/2,$$

$$\langle 2|e^{-i\alpha J_x}|1\rangle = -i\sin(\alpha)[1+\cos(\alpha)]/2,$$

$$\langle 2|e^{-i\alpha J_x}|-1\rangle = -i\sin(\alpha)(\cos(\alpha)-1)/2,$$

$$\langle 1|e^{-i\alpha J_x}|2\rangle = -i\sin(\alpha)[\cos(\alpha)+1)/2,$$

$$\langle 1|e^{-i\alpha J_x}|-2\rangle = -i\sin(\alpha)[\cos(\alpha-1)]/2.$$

In the odd-parity subspace, we then find

$$\langle\tilde{2}|e^{-i\alpha J_x}|\tilde{2}\rangle = \cos(\alpha),$$

$$\langle\tilde{2}|e^{-i\alpha J_x}|\tilde{1}\rangle = -i\sin(\alpha),$$

$$\langle\tilde{1}|e^{-i\alpha J_x}|\tilde{2}\rangle = -i\sin(\alpha),$$

$$\langle\tilde{1}|e^{-i\alpha J_x}|\tilde{1}\rangle = \cos(\alpha).$$

Finally, the F matrix in the odd-parity subspace is given by

$$F = Ue^{-i\alpha J_x}U^\dagger e^{-i\alpha J_x} = \begin{pmatrix} 1 & 0 \\ 0 & 1 \end{pmatrix}.$$

Because F turns out to be a unit matrix, this directly demonstrates that the two eigenphases of F are both zero (because $e^{i0}=1$). Two odd-parity eigenstates hence cross each other at $\hbar_\eta = 2\pi/3$. The symmetry of the spectrum then indicates another crossing at $\hbar_\eta = 10\pi/3$. In addition, this proof shows that this crossing is independent of α, which is also confirmed by our numerical calculations. Our proof can also be extended to other cases with a rather small J, because thanks to Wigner, the rotational matrix elements can be analytically obtained.

[1] P. G. Harper, Proc. Phys. Soc. London, Sect. A **68**, 874 (1955); D. R. Hofstadter, Phys. Rev. B **14**, 2239 (1976).
[2] B. Simon, Commun. Math. Phys. **89**, 227 (1983); A. Avila and S. Jitomirskaya, Ann. Math. **170**, 303 (2009).
[3] For recent theoretical work related to Hofstadter's butterfly spectrum in the context of two-dimensional electron systems, see N. Goldman, Phys. Rev. A **77**, 053406 (2008); J. Phys. B **42**, 055302 (2009).
[4] For general interest in quantum phase transitions, see S. Sachdev, *Quantum Phase Transitions* (Cambridge University Press, Cambridge, 2000).
[5] T. Geisel, R. Ketzmerick, and G. Petschel, Phys. Rev. Lett. **67**, 3635 (1991).
[6] J. Wang and J. B. Gong, Phys. Rev. A **77**, 031405(R) (2008).
[7] J. Wang, A. S. Mouritzen, and J. B. Gong, J. Mod. Opt. **56**, 722 (2009).
[8] D. W. Hone, R. Ketzmerick, and W. Kohn, Phys. Rev. A **56**, 4045 (1997).
[9] P. Leboeuf, J. Kurchan, M. Feingold, and D. P. Arovas, Phys. Rev. Lett. **65**, 3076 (1990).
[10] R. Lima and D. Shepelyansky, Phys. Rev. Lett. **67**, 1377 (1991); R. Artuso, G. Casati, and D. Shepelyansky, *ibid.* **68**, 3826 (1992); R. Ketzmerick, G. Petschel, and T. Geisel, *ibid.* **69**, 695 (1992).
[11] I. Dana, Phys. Lett. A **197**, 413 (1995).
[12] I. Dana and D. L. Dorofeev, Phys. Rev. E **72**, 046205 (2005).
[13] W. Lawton, A. S. Mouritzen, J. Wang, and J. B. Gong, J. Math. Phys. **50**, 032103 (2009).
[14] A. Eckardt, C. Weiss, and M. Holthaus, Phys. Rev. Lett. **95**, 260404 (2005); C. E. Creffield and T. S. Monteiro, *ibid.* **96**, 210403 (2006).
[15] (a) H. Lignier, C. Sias, D. Ciampini, Y. Singh, A. Zenesini, O. Morsch, and E. Arimondo, Phys. Rev. Lett. **99**, 220403 (2007); (b) E. Kierig, U. Schnorrberger, A. Schietinger, J. Tomkovic, and M. K. Oberthaler, *ibid.* **100**, 190405 (2008).
[16] M. P. Strzys, E. M. Graefe, and H. J. Korsch, New J. Phys. **10**, 013024 (2008).
[17] J. B. Gong, L. Morales-Molina, and P. Hänggi, Phys. Rev. Lett. **103**, 133002 (2009).
[18] Q. Zhang, P. Hänggi, and J. B. Gong, Phys. Rev. A **77**, 053607 (2008); New J. Phys. **10**, 073008 (2008).
[19] C. Weiss and T. Jinasundera, Phys. Rev. A **72**, 053626 (2005).
[20] M. Kohmoto, L. P. Kadanoff, and C. Tang, Phys. Rev. Lett. **50**, 1870 (1983); H. Hiramoto and M. Kohmoto, *ibid.* **62**, 2714 (1989); S. N. Evangelou and J.-L. Pichard, *ibid.* **84**, 1643 (2000); R. B. Diener, G. A. Georgakis, J. Zhong, M. Raizen, and Q. Niu, Phys. Rev. A **64**, 033416 (2001); A. M. García-García and J. Wang, Phys. Rev. Lett. **94**, 244102 (2005); see a recent review by F. Evers and A. D. Mirlin, Rev. Mod. Phys. **80**, 1355 (2008), and the references therein for quantum systems with multifractal wave functions at the critical Anderson transition point.
[21] F. Grossmann, T. Dittrich, P. Jung, and P. Hanggi, Phys. Rev. Lett. **67**, 516 (1991); G. Della Valle, M. Ornigotti, E. Cianci, V. Foglietti, P. Laporta, and S. Longhi, *ibid.* **98**, 263601 (2007)
[22] J. Wang and J. B. Gong, Phys. Rev. Lett. **102**, 244102 (2009).
[23] G. J. Milburn, J. Corney, E. M. Wright, and D. F. Walls, Phys. Rev. A **55**, 4318 (1997).
[24] J. Liu, W. Wang, C. Zhang, Q. Niu, and B. Li, Phys. Rev. A **72**, 063623 (2005); Q. Xie and W. Hai, Eur. Phys. J. D **33**, 265 (2005).
[25] F. Haake, *Quantum Signatures of Chaos* (Springer-Verlag, New York, 1992).
[26] See, for example, R. F. Fox and T. C. Elston, Phys. Rev. E **50**, 2553 (1994).
[27] J. B. Gong and J. Wang, Phys. Rev. E **76**, 036217 (2007).
[28] H. G. E. Hentschel and I. Procaccia, Physica D **8**, 435 (1983).
[29] V. S. Shchesnovich and V. V. Konotop, Phys. Rev. Lett. **102**, 055702 (2009).
[30] I. Guarneri and G. Mantica, Phys. Rev. Lett. **73**, 3379 (1994); R. Ketzmerick, K. Kruse, S. Kraut, and T. Geisel, *ibid.* **79**, 1959 (1997); F. Piéchon, *ibid.* **76**, 4372 (1996); G. Mantica, Electron. Trans. Numer. Anal. **25**, 409 (2006).
[31] E. M. Graefe, H. J. Korsch, and A. E. Niederle, Phys. Rev. Lett. **101**, 150408 (2008); D. Witthaut, F. Trimborn, and S. Wimberger, *ibid.*, **101**, 200402 (2008).
[32] G. Benenti, G. Casati, I. Guarneri, and M. Terraneo, Phys. Rev. Lett. **87**, 014101 (2001); I. Guarneri and M. Terraneo, Phys. Rev. E **65**, 015203(R) (2001); A. Tomadin, R. Mannella, and S. Wimberger, J. Phys. A **39**, 2477 (2006); A. Facchini, S. Wimberger, and A. Tomadin, Physica A **376**, 266 (2007).
[33] I. Guarneri and F. Borgonovi, J. Phys. A **26**, 119 (1993).
[34] R. N. Zare, *Angular Momentum* (Wiley, New York, 1987), p. 89.